RSC Advances

PAPER

Check for updates

Solid lipid nanoparticles as an effective sodium aescinate delivery system: formulation and anti-inflammatory activity

Jinyue Wang,[a] Hongyue Wang,[b] Hongjia Xu,[a] Jinghan Li,[c] Xu Zhang[b]
and Xiangrong Zhang [ID] *[ab]

Sodium aescinate-loaded solid lipid nanoparticles were fabricated using a melt-emulsification and ultrasonication method. Based on mean particle size, polydispersity index, and encapsulation efficiency, orthogonal and Box–Behnken designs were applied to optimize solid lipid nanoparticles with single emulsification and double emulsification methods. The characterization of solid lipid nanoparticles was investigated by X-ray diffractometry, differential scanning calorimetry, and scanning electron microscopy. After optimization of sodium aescinate-loaded solid lipid nanoparticles with single emulsification, the particle size was 90.7 nm and encapsulation efficiency was 76.5%. The sodium aescinate-loaded solid lipid nanoparticles with double emulsification were negatively charged spherical particles with the size of 109.4 nm and encapsulation efficiency up to 86.6%. Both solid lipid nanoparticles with single emulsification and double emulsification exhibited sustained release for 12 h without an initial burst release. The results indicated that sodium aescinate-loaded solid lipid nanoparticles by double emulsification showed more drug loading and stability after reconstitution. The sodium aescinate-solid lipid nanoparticles with double emulsification demonstrated stronger anti-inflammatory activity, including paw edema and ear swelling in mice than that of free sodium aescinate. Therefore, solid lipid nanoparticles have great potential as an effective sodium aescinate delivery system for application in medicine.

1. Introduction

Sodium aescinate (SA) is a triterpene saponin extracted from the dried fruits of *Aesculus wilsonii Rehd*. A number of studies have shown the therapeutic properties of SA, such as anti-inflammation,[1] anti-exudation,[2] detumescence,[3] and antioxidant effects;[4] it also can increase venous tension[5] and improve blood circulation.[6]

There are a few formulations of SA in clinical applications, including oral tablets, topical gel and injections.[7] However, SA is the hydrophilic sodium salt with poor lipophilic solubility and low oral bioavailability.[8] Thus, it is necessary to develop a new drug delivery system for SA with improved efficacy.

In recent years, nanomedicine has attracted increasing attention as a novel technology platform for enhancing bioavailability, reducing side effects, and controlling drug-

release properties. Commercially available nanomedicines include liposomes, micelles, nanosuspension, nano-emulsion, and nanoparticles.[9] Among the different nanoparticulate systems, solid lipid nanoparticles (SLNs) was made up of solid lipid core stabilized by surfactant at the interfacial region. Compared with traditional drug delivery systems, encapsulating drugs in SLNs can improve the bioavailability due to the physiological compatibility and biodegradability.[10–12] SLNs can carry hydrophilic as well as lipophilic active compound. The formulation of SLNs loaded with hydrophilic drug including zidovudine, insulin and diminazene were reported.[13] Usually, encapsulation of hydrophilic drugs is achieved by using double emulsification (DE) technique.[14] SLNs can be obtained by high-pressure homogenization, solvent evaporation, solvent emulsification, or ultrasonication technique.[15–17]

This study aimed to develop sodium aescinate – loaded solid lipid nanoparticles with single emulsification (SA-SLNs-SE) and double emulsification (SA-SLNs-DE) methods to increase the lipophilicity of SA, and therefore, improve the efficacy of SA as a potential anti-inflammatory candidate. SLNs were optimized by orthogonal and Box–Behnken design according to their mean particle size (PS), polydispersity index (PDI), and encapsulation efficiency (EE). X-ray diffractometry (XRD), differential scanning calorimetry (DSC), and scanning electron microscopy

a School of Traditional Chinese Materia Medica, Shenyang Pharmaceutical University, 103 Wenhua Road, Shenyang 110016, China. E-mail: zhangxr@vip.sina.com; Fax: +86-24-23986522; Tel: +86-24-23986522

b School of Function Food and Wine, Shenyang Pharmaceutical University, 103 Wenhua Road, Shenyang 110016, China

c Department of Pharmaceutics, College of Pharmacy, University of Minnesota-Twin Cities, 308 SE Harvard St, Minneapolis, 55455, Minnesota, USA

(SEM) were used to characterize the SLNs. The stability of SLNs was evaluated by the polydispersity, zeta potential, and transmission electron microscopy (TEM). In addition to the study of *in vitro* drug release, the anti-inflammatory effect of the SLNs formulations on mice were also investigated.

2. Materials and methods

2.1 Materials

Sodium aescinate (SA) was purchased from Nanjing Chunqiu Biological Engineering Co., Ltd. Glycerol monostearate (GMS) of the analytical grade was purchased from the Damao Chemical Reagent Factory of China. Egg yolk lecithin (EL) was purchased from Lipoid GmbH of Germany. Poloxamer 188 (F 68) was purchased from BASF of Germany. Anhydrous ethanol, methanol, and acetonitrile were procured from Concord of China. Other reagents were of HPLC or analytical grade.

2.2 Preparation of SA-SLNs-SE

SA was dissolved in ethanol at 75 °C and mixed with GMS and EL, which acted as the lipid phase. Simultaneously 20 mL aqueous solution of F 68 was kept at 75 °C as the aqueous phase. The aqueous phase was added to the lipid phase drop by drop and emulsified for 20 minutes to obtain a single emulsion (O/W). Finally, the emulsion was ultrasonicated under an ice bath for 12 min at 95% amplitude in a pulse regime (3 s on, 3 s off) using the ultrasonic probe processor (200 W, Nanjing Xianou, China). This emulsion was kept at 4 °C for 5 min to promote solidification of SA-SLNs-SE.

2.3 Preparation of SA-SLNs-DE

The SA aqueous solution acted as the internal aqueous phase, GMS and EL were heated above its melting point in ethanol as lipid phase. The internal aqueous phase into the lipid phase and the mixture was sonicated by an ultrasonication (Kunshan ultrasonic instrument, China) for 5 minutes at 75 °C to form the first emulsion (W/O). F 68 aqueous solution was kept at 75 °C as the external aqueous phase. The external aqueous phase was added to the lipid phase dropwise and emulsified for 15 minutes to form the W/O/W emulsion. Finally, the ultrasonic operation and cooling steps of SA-SLNs-DE were the same as that of SA-SLNs-SE.

2.4 Physicochemical characterization analyses of SLNs

The particle size was determined by laser diffraction on a Master sizer 2000 (Malvern Instruments, UK). PDI was obtained by dynamic light scattering (DLS) on the Zeta sizer Nano ZS 90 (Malvern Instruments, UK). Zeta potential (ZP) was determined by Laser Doppler Micro-electrophoresis equipment. All measurements were carried out in triplicate.

EE of all formulations was determined by measuring the concentration of the non-encapsulated drug in the solution.[18] In order to assess EE, a suitable volume (4 mL) of the final SLNs was placed in Microcon® centrifugal filters (50 kDa, Merck Millipore, USA). After centrifuge, the concentration of free SA was assayed by the HPLC-UV method. Similarly, the total SA

content was determined after destroying emulsification by methanol. The following equation was applied to confirm the percentage SA incorporated with SLNs:

$$EE(\%) = \frac{W_{total} - W_{free}}{W_{total}} \times 100\% \tag{1}$$

W_{total}: total weight of sodium aescinate in SLNs.
W_{free}: weight of free sodium aescinate in SLNs.
The drug loading (DL) was calculated as follows:

$$DL(\%) = \frac{W_{total} - W_{free}}{W_{lipid}} \times 100\% \tag{2}$$

W_{total}: total weight of sodium aescinate in SLNs.
W_{free}: weight of free sodium aescinate in SLNs.
W_{lipid}: lipid (GMS and EL) weight in SLNs.

2.5 Transmission electron microscopy

The morphology of the optimized SA-SLNs-SE and SA-SLNs-DE were analyzed by transmission electron microscopy (TEM) (JEM-2100F, Japan). The reconstituted SLNs suspension was put on a carbon-coated copper grid, and then a drop of 2% phosphotungstic acid was placed on a layer of SLNs. After staining for 5 min, excess dye was removed from the edge by filter paper. It was dried at room temperature for about half an hour, and the sample was evaluated for the TEM investigation at 100 kV.

2.6 X-ray diffractometry

SA, physical mixture, SA-SLNs-SE, and SA-SLNs-DE freeze-dried powder were respectively filled into the dishes of X-ray diffractometer (XRD) (X'Pert PRO MPD, Netherlands), using Ni-filter, CuKα radiation, 40 kV voltage and 40 mA current, scanning at a rate of 4° min^{-1} within the 2θ range of 5°–90°.

2.7 Differential scanning calorimetry

SA, physical mixture, SA-SLNs-SE, and SA-SLNs-DE freeze-dried powder were placed in an aluminum crucible of differential scanning calorimeter (DSC) (200F3 Maia®, Germany), and an empty crucible was set as a reference cell. The conditions were as follows: the heating rate is 10 °C min^{-1}; the scanning range is 30–230 °C with 30 mL min^{-1} nitrogen flow.

2.8 Scanning electron microscopy

The lyophilized powders of SA-SLNs-SE and SA-SLNs-DE were sprayed with gold and then the surface morphology was observed by a scanning electron microscope (SEM) (S4800, Japan). The voltage of microscope was operated at 5 kV for observation.

2.9 High-performance liquid chromatography analysis of SA

The chromatographic analysis was performed by L-7000 high-performance liquid chromatography (HPLC) (Hitachi, Japan) with an L-7420 UV-VIS Detector (Hitachi, Japan). The chromatographic separation was performed in a Diamonsil C$_{18}$

(250 mm × 4.6 mm, 5 μm, DIKMA) column. The mobile phase was consisted of acetonitrile and phosphoric acid solution (4 mL 80% phosphoric acid was added to 1000 mL distilled water), and the ratio was 40 : 60. The system was operated isocratically at a 1.0 mL min^{-1} flow rate, and UV absorbance was detected at a wavelength of 278 nm. The samples were filtered using a 0.22 μm membrane before their injection.

2.10 *In vitro* release study of sodium aescinate

The release study of SA from SLNs was evaluated by the dialysis bags method. Experiments were performed with 5 mL containing sodium aescinate-loaded nanoparticles suspension equivalent to a SA concentration of 15 mg mL^{-1}. The dialysis was achieved through a membrane (MW 20000, VAKE, USA) into 45 mL pH 7.4 PBS buffer, stirring at 100 rpm at 37 °C under magnetic stirrer (Yuhua instrument, China). At regular time intervals, 1.0 mL solution was drawn and 20 μL was injected for HPLC assay after filtered with 0.22 μm membrane. The release solution was replenished with 1.0 mL fresh phosphate buffer. 75 mg SA was accurately weighed and dissolved in 5 mL water to investigate the release of SA aqueous solution. All experiments were performed in triplicate. The cumulative release amounts of SA *versus* time were plotted and the data were fitted to the release kinetic models.

2.11 The stability study of SA-SLNs-SE and SA-SLNs-DE

The accelerated stability of the optimized SA-SLNs-SE and SA-SLNs-DE formulations was evaluated by WD-2A Drug Stability Tester (Jingtuo instrument technology, China). Three batches of SA-SLNs-SE and SA-SLNs-DE were placed at 40 °C and 75% relative humidity (RH) for three months. The formulations were assessed in terms of appearance, particle size, polydispersity, and encapsulation efficiency.

2.12 Anti-inflammatory activity of SA-SLNs-DE

2.12.1 Reagents and animals. Aspirin enteric-coated tablets were purchased from Ojina Pharmaceutical Co. Ltd of China. Kunming male mice weighing (20 ± 2) g were obtained from the experimental animal center of Shenyang Pharmaceutical University. The animals were allowed free access to standard feed and water ad libitum and were kept in clean cages filled with sawdust, which was replaced every three days. All experimental procedures were in accordance with the Guide for the Care and Use of Laboratory Animals and approved by the Animal Ethics Committee of Shenyang Pharmaceutical University.

2.12.2 Carrageenan-induce mice paw edema. Sixty male mice were randomly divided into six groups. SA aqueous solution (0.26 mg/20 g) was used as SA group. Blank SLNs group (0.2 mL/20 g) and aspirin drug group (0.26 mg/20 g) were used as control and positive groups,[19] and the remaining three groups obtained three kinds of SA-SLNs-DE (low, medium and high dose group, 0.2 mL/20 g). The contents of SA in the low, medium and high groups were 10, 60, and 100 mg/20 mL. The mice were administered by gavage once a day for 10 consecutive days. After the final one-hour administration of samples, the left hind paw edema was induced with an intraplantar injection

of 0.1 mL carrageenan solution (1%). The edema thickness of the sole was measured using a vernier caliper at 0, 1, 2, 3, 4, 5, and 6 h after carrageenan injection, and the difference of the double paws thickness was the degree of paw swelling. The paw swelling rate was calculated from the equation given below:

$$FR(\%) = \frac{TH_l - TH_r}{TH_l} \times 100\%$$

TH$_l$: the thickness of left paw (mm).
TH$_r$: the thickness of right paw (mm).

2.12.3 Xylene-induced ear swelling. Sixty male mice were assigned and administrated according to section "2.12.2". On the 10th day, 1 h after administration, xylene (50 μL) was wiped on the inner and outer sides of each mouse's right ear with a micropipette. The left ear was considered as a control. After 20 min of swelling, the mice were sacrificed, and the two ears were taken in the same position with a 7 mm hole punch and weighed. The poor quality of the double ears was the degree of ear swelling. The ears swelling rate was calculated as follows:

$$ER(\%) = \frac{W_r - W_l}{W_l} \times 100\%$$

W$_l$: the weight of left ear (mg).
W$_r$: the weight of right ear (mg).

2.12.4 Statistical analysis. SPSS Statistics 22.0 software was employed for data processing. One-way analysis of variance was executed for comparison between more groups. LSD *t*-test was used for comparison between two groups. The analysis was performed by OriginPro 8.0 software. A value $P < 0.05$ was considered statistically significant.

3. Results and discussion

3.1 Optimal formulation of SA-SLNs-SE

Taguchi method L9-type orthogonal array design was applied to optimize the formulation.[20] EE is an essential factor for evaluation of SLNs. GMS, EL, F 68, and drug lipid ratio were screened by the value of EE. It is an essential index for quality control of liposomes and nanoparticles to reflect the extent of drug encapsulation.[21] GMS, EL, F 68, and drug lipid ratio was represented by A, B, C, and D, respectively. The weight of A was 100, 200, and 300 mg; B was 300, 400, and 500 mg; C was 400, 500, and 600 mg. The ratio D was 1 : 5, 1 : 10, and 1 : 15. The encapsulation efficiency ranged from 71.0% to 86.4% by orthogonal test design (Table 1), and the degree of influence of various factors on the encapsulation efficiency of SA-SLNs was A > B > D > C.

According to the results of variance analysis, A, B and D exhibited a significant influence on the encapsulation efficiency ($P < 0.05$), while C had no significant impact on the encapsulation efficiency ($P > 0.05$). After a comprehensive analysis, $A_2B_2C_3D_2$ were chosen as the optimal formulation.

3.2 Optimal formulation of SA-SLNs-DE

Box–Behnken design (BBD) was employed for the prediction and development of an optimum SA-loaded SLNs.[22] Three

Table 1 L 9-type orthogonal test design and results for SA-SLNs-SE

No.	A	B	C	D	EE (%)
1	1	1	1	1	70.99
2	1	2	2	2	79.82
3	1	3	3	3	77.46
4	2	1	2	3	82.33
5	2	2	3	1	84.88
6	2	3	1	2	86.39
7	3	1	3	2	82.19
8	3	2	1	3	83.42
9	3	3	2	1	81.08
$\bar{K}_1$	76.090	78.503	80.267	78.983	
$\bar{K}_2$	84.533	82.707	81.077	82.800	
$\bar{K}_3$	82.230	81.643	81.510	81.070	
R	8.443	4.204	1.243	3.817	

Table 2 Composition of Box–Behnken design for SA-SLNs-DE formulations and observed values of the studied responses

No.	A	B	C	PS (nm)	EE (%)
1	100	300	500	112.5	69.67
2	300	300	500	269.5	71.40
3	100	500	500	126.1	74.36
4	300	500	500	129.7	80.49
5	100	400	400	142.7	73.37
6	300	400	400	224.4	76.94
7	100	400	600	95.55	72.24
8	300	400	600	226.3	75.46
9	200	300	400	181.1	87.00
10	200	500	400	111.7	79.35
11	200	300	600	172.9	69.65
12	200	500	600	110.1	79.03
13	200	400	500	165.4	73.61
14	200	400	500	148.6	71.91
15	200	400	500	116.6	74.81
16	200	400	500	122.0	75.11
17	200	400	500	119.3	73.25

factors were the amount of GMS, EL, and F 68. The high, medium, and low levels of each factor were represented by 1, 0, and −1. The investigated responses were PS (nm) and EE (%). BBD design experiment established the mathematical model for optimized formulation and analysed by the software of Design Expert 8.0.7. GMS, EL, and F 68 were represented by A, B, and C, respectively. The amount of A was 100, 200, or 300 mg; B was 300, 400, or 500 mg; C was 400, 500, or 600 mg. Totally 17

formulations were prepared according to the BBD with minimum PS and maximum EE, which were displayed in Table 2.

The PS is a crucial character that influences the properties of SLN.[23] SLNs with a particle size around 100 nm and narrow size distribution are desirable. Therefore, particle size was first analyzed by Design Expert 8.0.7 software. The fitting equation was described as following:

$$PS = 134.38 + 46.63A - 32.30B - 6.88C - 38.35AB + 12.26AC + 1.65BC + 26.68A^2 - 1.61B^2 + 11.18C^2$$

The results implied that the quadratic model was significant. The P values of A, B, AB, and A^2 were all less than 0.05, suggesting that they had a considerable influence on the PS of SLNs. In general, the F-value test showed that the total model equation was significant ($P < 0.05$, $R^2 = 0.9390$), and GMS (A) had the most critical influence on PS, followed by EL (B). The analysis results of the 3D regression model were shown in Fig. 1.

EE was analyzed by Design Expert 8.0.7 software. The fitting equation was obtained:

$$EE = 73.74 + 1.83A + 1.94B - 2.54C + 1.10AB - 0.087AC + 4.26BC - 2.01A^2 + 2.25B^2 + 2.77C^2$$

The P values of C and BC were both less than 0.05, indicating that they had a significant influence on the EE (%) of SLNs. The F-value test presented that the total model equation was significant ($P < 0.05$, $R^2 = 0.8271$), and F 68 (C) had the most important influence on EE, followed by EL (B). The results of the 3D regression model analysis were presented in Fig. 2.

According to the response surface, the difference between the two factors was significant with the larger curvature of the 3D interaction surface. The optimal formulation was analyzed and predicted by Design Expert 8.0.7 software. The optimal formulation of 20 mL SA-SLNs-SE was consisted of 60 mg SA, 200 mg GMS, 400 mg EL, and 600 mg F 68. The optimal 20 mL SA-SLNs-DE contained 60 mg SA, 204 mg GMS, 500 mg EL, and 600 mg F 68. The predicted diameter of SA-SLNs-DE was 107.3 nm and 82.5% of EE. Three batches of samples were obtained for verification. The actual values of diameter and EE were 109.4 ± 0.8 nm and 86.6 ± 0.8%, respectively. The results suggested that the deviation values of particle size and
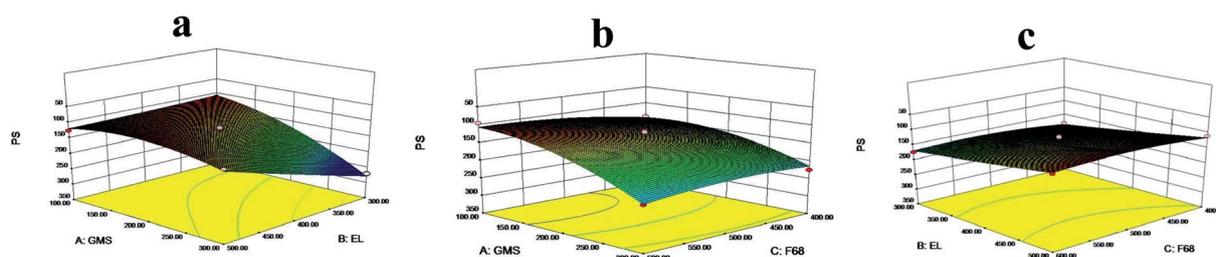

Fig. 1 Response 3D plots of interaction on PS (a) GMS *versus* EL (b) GMS *versus* F 68 (c) EL *versus* F 68.
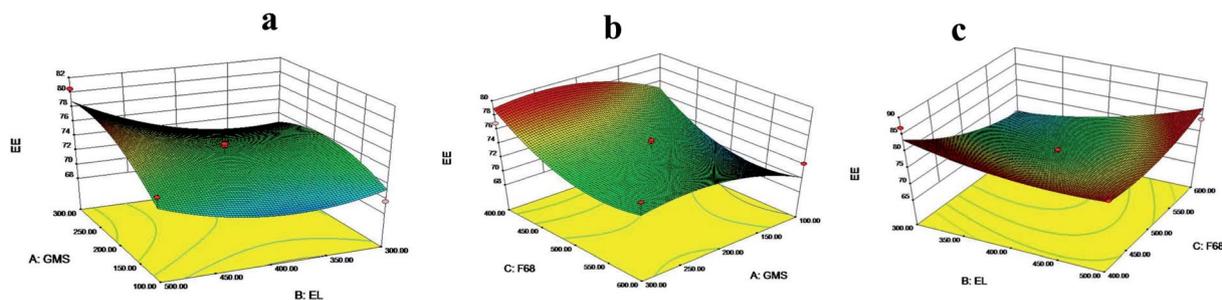
Fig. 2 Response 3D plots of interaction on EE (a) GMS *versus* EL (b) F 68 *versus* GMS (c) EL *versus* F 68.

encapsulation efficiency were less than 5%, so the optimal formulation was suitable for SA-SLNs-DE.

3.3 Characterization of reconstituted SA-SLNs-SE and SA-SLNs-DE

The appearance of SA-SLNs-SE and SA-SLNs-DE was a uniform liquid with milky white and light blue opalescence. After dilution, the liquid became near-clear liquid with blue opalescence. SA-SLNs-SE and SA-SLNs-DE have the same appearance and no sediment.

The particle size and PDI of SA-SLNs-SE were (90.7 ± 0.2) nm and (0.236 ± 0.015), while those of SA-SLNs-DE were (109.4 ± 0.8) nm and (0.283 ± 0.024). The particle size of both nanoparticles was in the nanoscale range, and the PDI was uniform for nanomedicine. The potential values of SA-SLNs-SE were (−0.28 ± 0.01) mV, and the potential value of SA-SLNs-DE was (−31.50 ± 0.02) mV. When the absolute value of potential value is greater than 30 mV, electrostatic repulsion enables the existence of nanoparticles to be stable and without precipitation phenomenon of particles due to aggregation.[24,25] SA-SLNs-DE may be more stable than that of SA-SLNs-SE according to the zeta potential analysis. According to the TEM images in Fig. 3, the more negative zeta potential value of SA-SLNs-DE resulted in a less aggregated colloid system, while SLNs fabricated by single emulsification were found with aggregated clusters.

The pH value of SA-SLNs-SE and SA-SLNs-DE were 7.13 and 6.87, respectively. The Chinese Pharmacopoeia suggests that the pH value for the injection is 4–9, both of which are within the range. The preparation was also stable at this pH value according to previous reports.[26,27] Encapsulation efficiency of SA-SLNs-SE and SA-SLNs-DE were 76.5% and 86.6%, and drug loading were 8.7% and 10.7%, respectively. The encapsulation efficiency and drug loading of SA-SLNs-DE were higher than SA-SLNs-SE, indicating that SA-SLNs-DE had a better drug loading capacity than SA-SLNs-SE. According to the above results, the double emulsification method is better than that of the single emulsification method. This also complied with previous report on encapsulate hydrophilic drugs by w/o/w emulsion.[28]

3.4 XRD, DSC and SEM of SA-SLNs-SE and SA-SLNs-DE

The optimized SA-SLNs-SE and SA-SLNs-DE formulations were freeze-dried. As a saponin, the free SA is in amorphous form (Fig. 4). A similar amorphous state was also discovered in other saponins.[29,30] However, the unstable amorphous state may bring stability concerns during preparation and storage. Compared with free SA, the freeze-dried formulations have more diffraction peaks in the XRD pattern and additional melting endotherm around 165 °C, which are the characteristic feature of crystalline SA.[31] The lyophilized products showed needle-like crystals under SEM (Fig. 5). The crystallization of SA in the SLNs formulations contributed to the elegant appearance and potentially improved physical stability of the product.[32] In addition, due to the solubility advantage of the developed formulation, a uniform liquid of SLNs can be easily achieved within 30 seconds. Therefore, relevant characterizations were conducted in the liquid state.
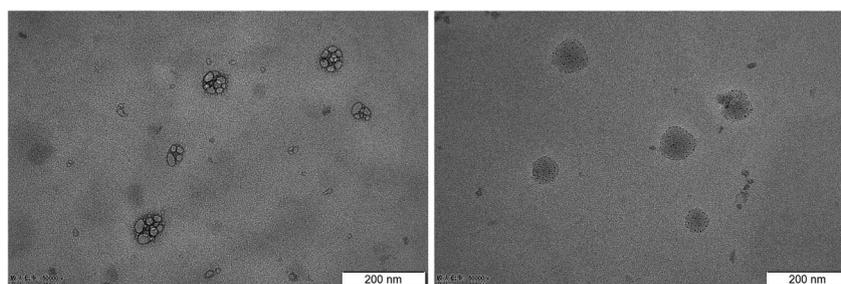

Fig. 3 TEM images of SA–SLNs–SE (left) and SA–SLNs–DE (right).
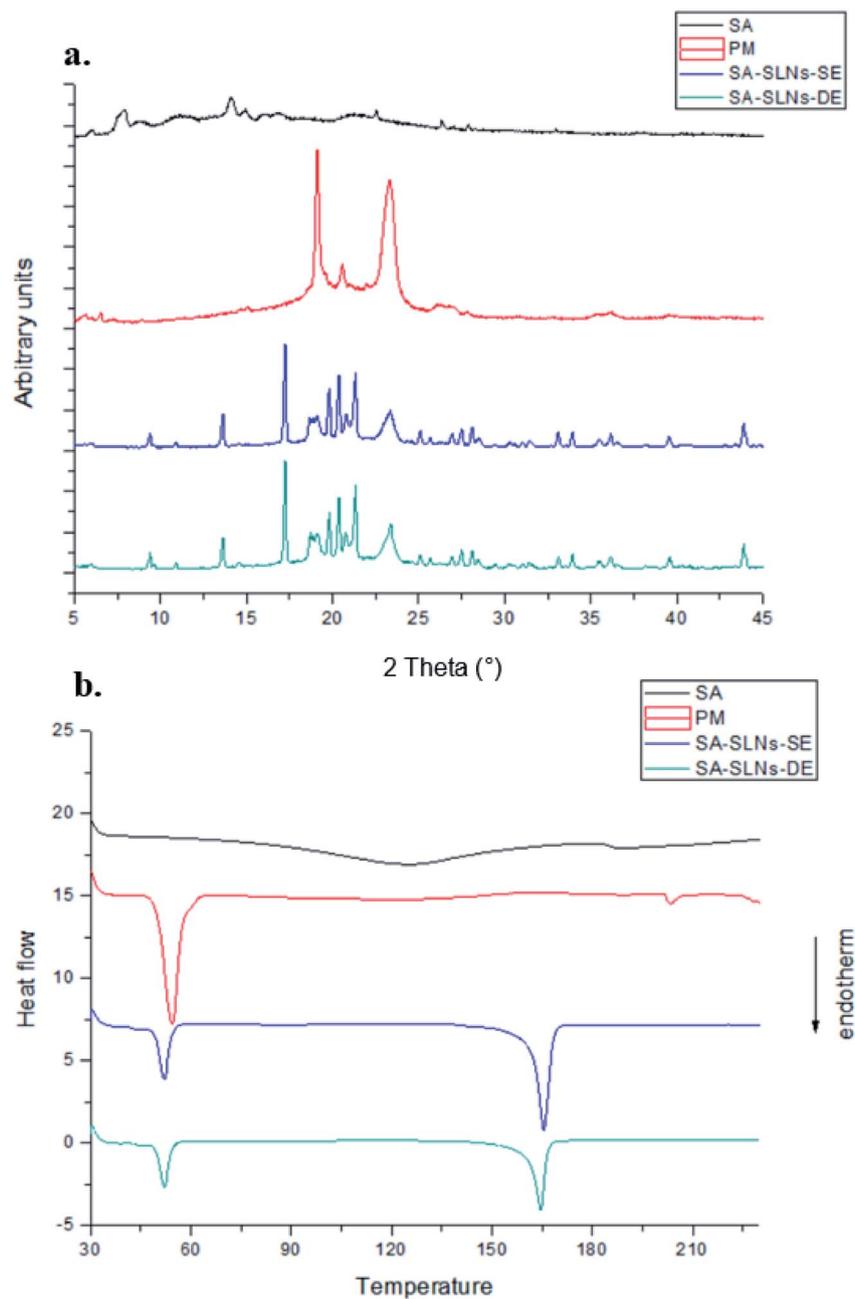
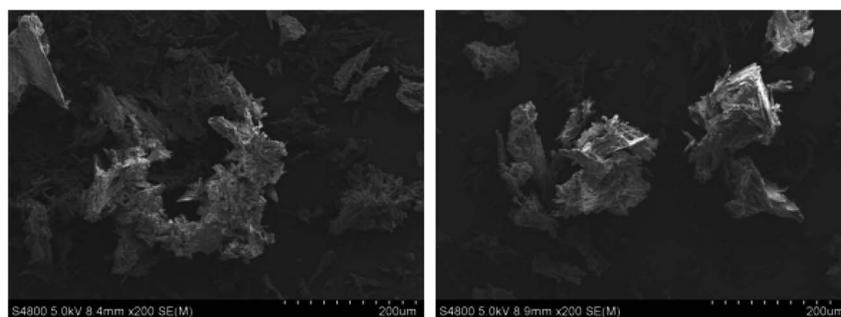Fig. 4 (a) XRD patterns and (b) DSC thermograms of SA, PM, SA-SLNs-SE, and SA-SLNs-DE.

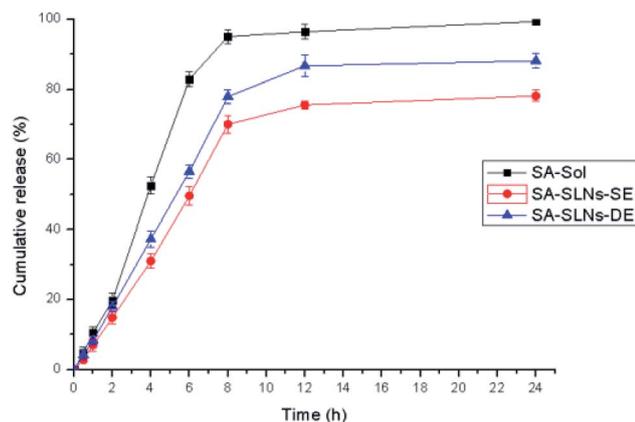Fig. 5 SEM of freeze-dried SLNs-SE (left) and SA-SLNs-DE (right).

Fig. 6 *In vitro* release profiles of SA-sol, SA-SLNs-SE and SA-SLNs-DE.

3.5 *In vitro* release study of sodium aescinate

SA is a hydrophilic drug and the pH of the SLNs solution is around 7.0, so pH 7.4 PBS was taken as the *in vitro* release medium for the study. The release curves were different significantly from sodium aescinate water solution (SA-sol), SA-SLNs-SE, and SA-SLNs-DE (Fig. 6). The cumulative release amount of SA-sol after 8 hours reached more than 95%. The cumulative release amount SA-SLNs-SE and SA-SLNs-DE were only 70.06% and 78.00% after 8 h, and the cumulative release amount reached 78.21% and 88.16% after 24 h. The release amount of SA from SA-SLNs-DE was higher than that of SA-SLNs-SE.

The release profiles were fitted into different kinetic models. The highest correlation coefficient ($r = 0.9427$) of SA-SLNs-SE

was found for the Higuchi model (Table 3). The highest correlation coefficient ($r = 0.9446$) of SA-SLNs-DE was also found for the Higuchi model. This model suggested the releases of drug were controlled by expansion and without an initial burst release. The drug loaded in SLNs was released slowly as the lipid material gradually dissolved.[33]

3.6 Accelerated stability study

The appearance, particle size, PDI, and encapsulation efficiency of the SA-SLNs-SE and SA-SLNs-DE were monitored under the condition of 40 °C and 75% RH for 3 months.

As shown in Table 4, SA-SLNs-SE and SA-SLNs-DE remained stable in the first month, but both formulations changed gradually at the second month. The appearance changed from milky to light yellow. The particle size increased gradually, but entrapment efficiency reduced significantly. Especially after three months, the SA-SLNs-SE and SA-SLNs-DE appeared pink, and the liquid became sticky. The results indicated that stability of SA-SLNs-DE was better than that of SA-SLNs-SE.

3.7 Anti-inflammatory activity of SA-SLNs-DE

3.7.1 Carrageenan-induced rat paw edema. Intraplantar injections of carrageenan provoked marked, time-related and progressive increases in the hind paw thickness of the control mice (control group) are shown in Fig. 7. There was a significant reduction in carrageenan-induced mice paw edema administered with SA-SLNs-DE from 1 to 6 h. After 2 hours of paw edema, the mice had the highest paw swelling rate on the sole, then decreased over time. Among the three groups of SA-SLNs-DE, the inhibition rate of the high dose group was the highest in mice, followed by the medium-dose group. Therefore, the anti-

Table 3 The model simulated for the release profiles of SA-SLNs-SE and SA-SLNs-DE

	SA-SLNs-SE		SA-SLNs-DE	
Model	Equation	r	Equation	r
Zero order	$R = 3.5922t + 13.611$	0.8527	$R = 4.0223t + 16.205$	0.8514
First order	$\ln(100 - R) = -0.102t + 4.4462$	0.8950	$\ln(100 - R) = -0.0723t + 4.4609$	0.9083
Higuchi	$R = 20.161t^{1/2} - 5.4687$	0.9427	$R = 22.655t^{1/2} - 5.3249$	0.9446
Ritger–Peppas	$\ln R = 1.1084 \ln t + 1.5359$	0.9045	$\ln R = 1.0734 \ln t + 1.7394$	0.8823
Hixon–Crowell	$(100 - R)^{1/3} = -0.087t + 4.4186$	0.8818	$(100 - R)^{1/3} = -0.1116t + 4.381$	0.8916

Table 4 The accelerated stability results of SA-SLNs-SE and SA-SLNs-DE

|		Time (month)			
Index		0	1	2	3
Appearance	SA-SLNs-SE	Milky	Milky	Light yellow	Pink
	SA-SLNs-DE	Milky	Milky	Light yellow	Pink
PS (nm)	SA-SLNs-SE	90.7 ± 0.2	185.7 ± 0.4	327.6 ± 0.6	583.9 ± 1.2
	SA-SLNs-DE	109.4 ± 0.8	178.2 ± 0.2	280.5 ± 0.4	416.2 ± 0.8
PDI	SA-SLNs-SE	0.236 ± 0.015	0.327 ± 0.012	0.518 ± 0.011	0.621 ± 0.005
	SA-SLNs-DE	0.283 ± 0.024	0.302 ± 0.017	0.386 ± 0.013	0.428 ± 0.012
EE (%)	SA-SLNs-SE	76.5 ± 2.2	72.3 ± 1.5	60.2 ± 2.2	43.0 ± 0.9
	SA-SLNs-DE	86.6 ± 2.0	82.4 ± 1.8	74.0 ± 1.3	58.5 ± 1.5
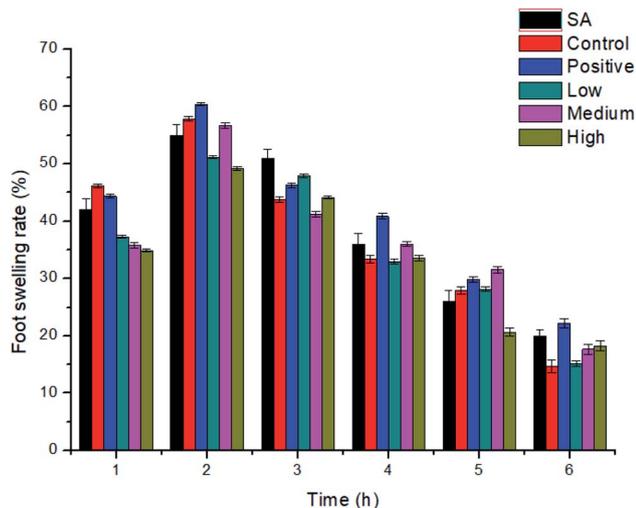
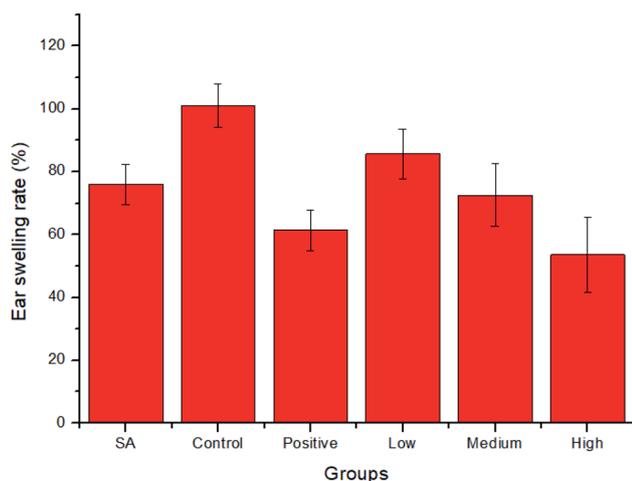**Fig. 7** The paw swelling rate of SA-SLNs-DE ($n = 10$).

Fig. 8 Ear swelling rate treated with various doses of SA-SLNs-DE ($n = 10$).

inflammatory effect was dose-dependent. Aspirin also significantly decreased the edema induced by carrageenan.

3.7.2 Xylene-induced ear swelling. The vehicle control group showed a marked increase in the weight of the ears and exhibited obvious inflammatory symptoms, including redness and swelling. SA decreased the weight of ears at a different group of SA-SLNs-DE and was statistically significant, as shown in Fig. 8. SA-SLNs-DE treated dose-dependently decreased xylene-induced ear edema in mice. The high dose group was more effective than aspirin. The results indicated that SA-SLNs had a potential anti-inflammatory effect on acute xylene-induced inflammation.

4. Conclusion

In the present research, two kinds of SLNs controlled SA release were optimized by orthogonal and Box–Behnken design. The prepared SLNs showed good attributes of low particle size and polydispersity. The encapsulation efficiency and drug loading of SA-SLNs-DE were higher than SA-SLNs-SE. SA-SLNs-DE possessed higher zeta potential showed that SLNs by the w/o/w method was more stable than that of SA-SLNs-SE. SA-SLNs-DE exhibited sustained release with the Higuchi model. The SA-SLNs-DE reduced inflammatory symptoms much effectively than that of free SA. This study provides valuable information by double emulsification to encapsulate a hydrophilic SA into solid lipid nanoparticles.

Conflicts of interest

The authors report no conflict of interest.

Acknowledgements

References

1 Z. Zhang, G. Cao, L. Sha, D. Wang and M. Liu, *Inflammation*, 2015, **38**, 1942–1948.
2 H. Hou, W. X. Li, X. Cui, D. C. Zhou, B. Zhang and X. P. Geng, *World J. Gastroenterol.*, 2019, **25**, 5483–5493.
3 L. Zhang, M. Fei, H. Wang and Y. Zhu, *Brain Res. Bull.*, 2020, **157**, 26–36.
4 Y. K. Wang, J. Han, W. J. Xiong, Q. Y. Yuan, Y. P. Gu and J. Li, *Molecules*, 2021, **17**, 10267–10275.
5 J. Liu, Y. Li, X. Yuan, Z. Yang and Z. Lin, *Med. Hypotheses*, 2008, **71**, 762–764.
6 L. Li, B. Xu, C. Li, M. M. Zhang, S. J. Wu and W. J. Dang, *Int. J. Ophthalmol.*, 2020, **13**, 1546–1553.
7 Y. Wang, Z. Ye, X. Hu, J. Huang and Z. Luo, *Injury*, 2010, **41**, 707–716.
8 X. Wu, L. Liu, M. Zhang, D. Wu, Y. Wang and Y. Sun, *J. Chromatogr. B: Anal. Technol. Biomed. Life Sci.*, 2010, **878**, 861–867.
9 H. Cabral and K. Kataoka, *J. Controlled Release*, 2014, **28**, 465–476.
10 Y. Pan, R. V. Tikekar and N. Nitin, *Int. J. Pharm.*, 2016, **511**, 322–330.
11 I. Cacciatore, M. Ciulla, E. Fornasari, L. Marinelli and A. Stefano Di, *Expert Opin. Drug Delivery*, 2016, **13**, 1121–1131.
12 F. Wang, M. Zhang, D. Zhang, Y. Huang, L. Chen and S. Jiang, *J. Biomed. Res.*, 2018, **6**, 411–423.
13 F. C. Wang, F. Peyronel and A. G. Marangoni, *Cryst. Growth Des.*, 2016, **16**, 297–306.
14 Y. Mirchandani, V. B. Patravale and S. Brijesh, *J. Controlled Release*, 2021, **335**, 457–464.
15 F. Ishii, T. Nii and J. Jan, *Soc. Food Sci.*, 2016, **63**, 363–368.
16 Y. Duan, A. Dhar, C. Patel, M. Khimani, S. Neogi and P. Sharma, *RSC Adv.*, 2020, **10**, 26777–26791.

17 M. J. Ansari, M. K. Anwer, S. Jamil, R. Al-Shdefat, B. E. Ali and M. M. Ahmad, *Drug Delivery*, 2016, **23**, 1972–1979.

18 B. Rodenak-Kladniew, G. A. Islan, M. G. de Bravo, N. Durán and G. R. Castro, *Colloids Surf., B*, 2017, **154**, 123–132.

19 S. H. Sohn, T. S. Kim, J. W. Kim, S. M. Yoo and W. M. Jo, *Clin. Hemorheol. Microcirc.*, 2020, **77**, 435–442.

20 S. R. Youngren-Ortiz, D. B. Hill, P. R. Hoffmann, K. R. Morris, E. G. Barrett and M. G. Forest, *J. Aerosol Med. Pulm. Drug Delivery*, 2017, **30**, 299–321.

21 M. G. Fariba, H. Z. Ashrafalsadat, G. Fariba, E. H. Bahman, N. Fahimeh and S. Razi, *J. Liposome Res.*, 2018, **28**, 226–235.

22 G. Bina and V. Amber, *Artif. Cells, Nanomed., Biotechnol.*, 2016, **44**, 571–580.

23 A. J. Almeida and E. Souto, *Adv. Drug Delivery Rev.*, 2007, **59**, 478–490.

24 L. Guo, H. Chen, N. He and Y. Deng, *Chin. Chem. Lett.*, 2018, **29**, 1829–1833.

25 Q. Ye, T. Li, J. Li, L. Liu, X. Dou and X. Zhang, *J. Drug Delivery Sci. Technol.*, 2020, **56**, 101528.

26 Z. Li and X. Dai, *Int. J. Hydrogen Energy*, 2021, **46**, 26347–26357.

27 Y. Deng, K. Liu, S. Zhao and J. Sun, *Food and Drug*, 2018, **20**, 340–343.

28 M. Nabi-Meibodi, B. Navidi, N. Navidi, A. Vatanara, M. Reza Rouini and V. Ramezani, *J. Drug Delivery Sci. Technol.*, 2013, **23**, 225–230.

29 W. G. Ma, M. Mizutani, K. E. Malterud, S. L. Lu, B. Ducrey and S. Tahara, *Phytochemistry*, 1999, **52**, 1133–1139.

30 B. Shao, G. Qin, R. Xu, H. Wu and K. Ma, *Phytochemistry*, 1995, **38**, 1473–1479.

31 J. Jia, J. Wang, K. Zhang, D. Zhou, F. Ge and Y. Zhao, *J. Supercrit. Fluids*, 2017, **130**, 267–272.

32 C. Telang and R. Suryanarayanan, *Pharm. Res-Dordr.*, 2005, **22**, 153–160.

33 P. Costa and J. M. S. Lobo, *Eur. J. Pharm. Sci.*, 2001, **13**, 123–133.